JOURNAL OF GEOPHYSICAL RESEARCH, VOL. 99, NO. B11, PAGES 21,659–21,665, NOVEMBER 10, 1994

An in situ estimation of anisotropic elastic moduli for a submarine shale

Douglas E. Miller
Schlumberger-Doll Research, Ridgefield, Connecticut

Scott Leaney
Schlumberger Wireline and Testing, Jakarta, Indonesia

William H. Borland
Schlumberger Overseas, Bangkok, Thailand

Abstract. Direct arrival times and slownesses from wide-aperture walkaway vertical seismic profile data acquired in a layered anisotropic medium can be processed to give a direct estimate of the phase slowness surface associated with the medium at the depth of the receivers. This slowness surface can, in turn, be fit by an estimated transversely isotropic medium with a vertical symmetry axis (a "TIV" medium). While the method requires that the medium between the receivers and the surface be horizontally stratified, no further measurement or knowledge of that medium is required. When applied to data acquired in a compacting shale sequence (here termed the "Petronas shale") encountered by a well in the South China Sea, the method yields an estimated TIV medium that fits the data extremely well over 180° of propagation angles sampled by 201 source positions. The medium is strongly anisotropic. The anisotropy is significantly anelliptic and implies that the quasi-shear mode should be triplicated for off-axis propagation. Estimated density-normalized moduli (in units of km^2/s^2) for the Petronas shale are $A_{11} = 6.99 \pm 0.21$, $A_{33} = 5.53 \pm 0.17$, $A_{55} = 0.91 \pm 0.05$, and $A_{13} = 2.64 \pm 0.26$. Densities in the logged zone just below the survey lie in the range between 2200 and 2400 kg/m^3 with an average value close to 2300 kg/m^3.

Introduction

In any horizontally layered medium (i.e., a medium which is invariant under all horizontal coordinate transformations $(x, y, z) \rightarrow [x + a, y + b, z)]$, propagation (for any type of wave) between any two points (say (x_1, y_1, z_1) and (x_2, y_2, z_2)) must depend only on their two depths and their relative offsets (i.e., on $(z_1, z_2, x_2 - x_1, y_2 - y_1)$). It follows that a seismic experiment made in such a medium with a vertical array in a borehole and multiple (identical) sources along a line on the surface (such as a walkaway vertical seismic profile (VSP)) is fully equivalent to an experiment made with a single source and a two-dimensional array of subsurface receivers.

This simple observation formed the basis for the method of wave fronts [*Ansel*, 1931; *Thornberg*, 1930]. Various authors who used the method observed that p wave propagation was sometimes anisotropic, particularly in shales [*Ricker*, 1953; *Hagedoorn*, 1954; *Jolly*, 1956; *Dunoyer de Segonzac and Laherrere*, 1959; *Meisner*, 1961; *Vander Stoep*, 1966].

The most popular methods used in attempting to quantify the anisotropy have been based on layer stripping, assuming that the medium is layered and, at least approximately, elliptical for p waves [*Cholet and Richard*, 1954; *Dunoyer de Segonzac and Laherrere*, 1959; *Vander Stoep*, 1966; *Byun et al.*, 1989; *Byun and Corrigan*, 1990].

White et al. [1983] made VSP measurements in two closely spaced boreholes in the Pierre shale formation to obtain both vertical and horizontal components of phase slowness for direct arrivals generated at eight surface locations. These phase slowness data were fit by a transversely isotropic anisotropic medium with a vertical symmetry axis (a "TIV" medium) under an assumption of mild anisotropy.

In a layered medium, the method of wave fronts can provide data analogous to that of *White et al.* [1983] but derived from measurements in a single borehole. *Gaiser* [1990] observed that partial derivatives of arrival time with respect to source offset and receiver depth (i.e., the gradient of times contoured in a classical wave front chart) directly give points lying on the phase slowness surface of the medium at the depth of the receivers. *Brodov et al.* [1984] showed anisotropic phase diagrams that may have been computed by a similar method. *Gaiser* [1990] used the method to analyze a multioffset VSP data set from east Texas, fitting measured phase points with linearized TIV phase slowness functions in a style similar to that of *White et al.* [1983].

Miller and Spencer [this issue] show that the linearization step in the inversion from phase slowness data to elastic parameters can be omitted in favor of a direct regression based on an algebraic rearrangement of the medium's dispersion equation.

Paper number 94JB01849.
0148-0227/94/94JB-01849$05.00

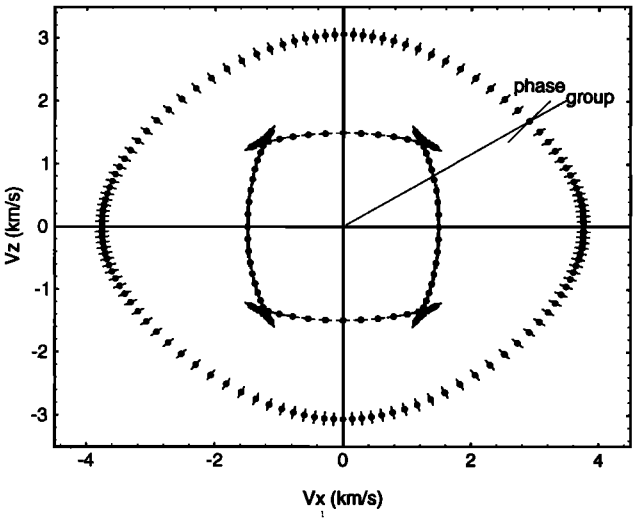

Figure 1. Group velocity surface associated with the Greenhorn shale as measured by *Jones and Wang* [1981]. Points are sampled uniformly as a function of phase angle. Tickmarks indicate polarization directions.

In this paper, we analyze wide-aperture walkaway VSP data recorded at an offshore well in the South China Sea. A variant of Gaiser's method is used to obtain qP phase slowness points from over 200 source positions for a single receiver depth in a compacting shale. These phase slowness points are fit by a transversely isotropic model using the method described by *Miller and Spencer* [this issue]. The estimated TIV medium fits the data extremely well over a full range of vertical propagation angles. The medium is strongly anisotropic. The anisotropy is significantly anelliptic and implies that the quasi-shear mode should be triplicated for off-axis propagation.

Anisotropy 101

Figure 1 shows the impulse response (group velocity surface) for a representative shale medium. The medium is transversely isotropic (TIV) with a vertical axis of symmetry. For the inplane strain modes shown here, propagation is controlled by four density-normalized elastic moduli $\{A_{11}, A_{13}, A_{33}, A_{55}\}$ [e.g., *Helbig and Schoenberg*, 1987]. In this case the values have been taken from the Greenhorn shale of *Jones and Wang* [1981] and are {14.17, 4.42, 9.38, 2.23}, all in units of km^2/s^2.

All points on the surface have the same travel time from the origin. At each point, the phase direction is normal to the surface, the group direction passes through the origin, and the attached tickmark shows the associated polarization direction. The points are sampled uniformly in phase angle. The outer surface is the quasi-P surface (polarization is approximately parallel to phase direction); the inner surface is the quasi-S surface (polarization is approximately normal to phase direction). If we write $T(x, z)$ for the travel time of the quasi-P wave to the point (x, z), then $S_z = \partial T/\partial z$ and $S_x = \partial T/\partial x$ are the vertical and horizontal components of the phase slowness vector [e.g., *White et al.*, 1983; *Gaiser*, 1990].

The shape of the surface is determined from the density-normalized moduli by the requirement that each phase slowness point (S_x, S_z) satisfy the dispersion equation (here for both the wave vector and the strain in the x-z plane):

$$A_{11}A_{55}X^2 + A_{33}A_{55}Z^2 + AXZ - (A_{11} + A_{55})X - (A_{33} + A_{55})Z + 1 = 0, \quad (1)$$

where

$$A = A_{11}A_{33} + A_{55}^2 - (A_{13} + A_{55})^2,$$

$$(X, Z) = (S_x^2, S_z^2).$$

The collection of all phase slowness points forms the phase slowness surface. It is the polar reciprocal of the group velocity surface.

Vertical P velocity is given by $V_{33} = (A_{33})^{1/2}$, horizontal P velocity by $V_{11} = (A_{11})^{1/2}$; axial shear velocity is $V_{55} = (A_{55})^{1/2}$. Quasi-P velocity near 45° is approximately given by $V_{qp} = (A_{qp})^{1/2}$, where

$$A_{qp} = [A_{11} + A_{33} + 2(A_{13} + 2A_{55})]/4.$$

Quasi-S velocity near 45° is approximately given by $V_{qs} = (A_{qs})^{1/2}$, where

$$A_{qs} = (A_{11} + A_{33} - 2A_{13})/4.$$

The approximations are exact when $A_{11} = A_{33}$ (i.e., in a TIV medium with cubic symmetry). In an isotropic medium,

$$A_{11} = A_{33} = A_{qp} = (\lambda + 2\mu)/\rho$$

and

$$A_{55} = A_{qs} = \mu/\rho.$$

The qSV slowness surface is circular (i.e., isotropic) exactly in the case where the qP surface is elliptical. This is equivalent to the requirement that the qP and qSV squared slownesses defined implicitly by (1) lie on straight lines. The algebraic condition for this is that

$$A_{13} + 2A_{55} = (A_{11} + A_{33})/2. \quad (2)$$

Equivalent algebraic conditions are $A_{qp} = (A_{11} + A_{33})/2$ and $A_{qs} = A_{55}$. It is, therefore, natural to quantify the anellipticity using either the qP velocity ratio $V_{qp}/[(A_{11} + A_{33})/2]^{1/2}$ or the qSV velocity ratio V_{qs}/V_{55}. In the case of the Greenhorn shale, these ratios have values 0.88 and 1.28, respectively.

The most striking feature of Figure 1 is the triplication of the qSV wave which is associated with the substantial failure of (2). This type of pattern has been seen in numerous laboratory studies [cf. *Thomsen*, 1986] and in a few field studies [e.g., *Vander Stoep*, 1966; *Miller and Chapman*, 1991]. It will be seen in the present analysis. It can be associated with lack of resistance to slip along horizontal planes [*Schoenberg and Douma*, 1988]. *Dellinger* [1990] discusses an algebraic condition for the presence of qSV triplication. Since the failure of (2) is detectable as anellipticity of the qP surface, it is possible to obtain qualitative information about the qSV surface from accurate qP measurements alone. *Miller and Spencer* [this issue] show that for the Petronas shale medium described in the present paper, qSV triplication is present in virtually any TIV medium consistent with the measured qP slowness values.

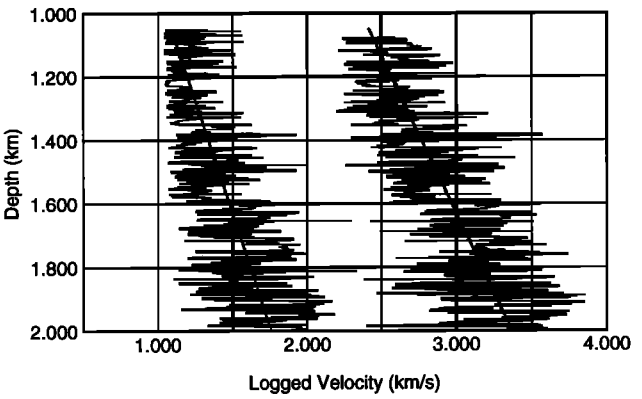

Figure 2. Shear and compressional sonic logs recorded below the receiver interval. Superimposed on the logs are lines defined by the equations $V = 0.358 + 0.7D$ and $V = 1.369 + 1.0D$.

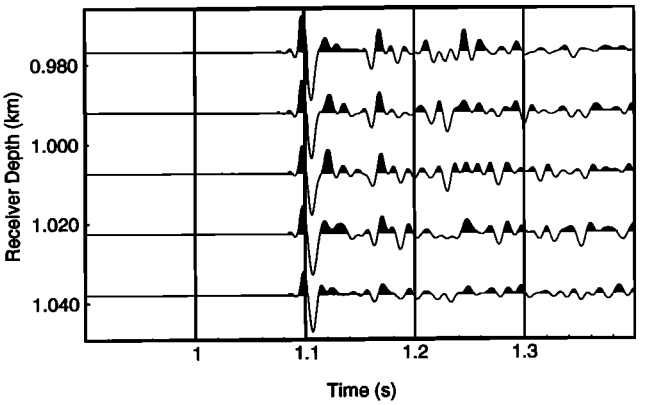

Figure 4. Radial component common source gather for the source at −1.985 km offset from the well.

Field Study

A wide-aperture walkaway VSP survey was acquired using the Schlumberger five-level three-component array seismic imager tool positioned with receiver depths from 0.978 to 1.038 km. A marine air gun source occupied positions from −3.000 to +4.000 km offset.

The well was drilled from an offshore platform into a Tertiary sand-shale sequence with a normal compaction trend. Compressional and shear sonic logs run between depths 1.100 m and 2.000 km showed gradient velocity trends of about 1.0 and 0.7 s^{-1}, respectively, with substantial variation around the trends (Figure 2).

Figure 3 shows selected vertical component traces from the receiver at $z_3 = 1.008$ km. The data display a high degree of symmetry about zero offset, suggesting that the medium is horizontally layered. The amplitude of the first arrival on the vertical component goes to zero at offsets of about 2.000 km on each side. At these "turning" offsets, the apparent vertical velocity as seen on common shot gathers is infinite, indicating that first arrivals from these offsets are horizontal (turning) P waves (Figure 4).

Vertical component traces from a common shot made close to the well indicate a vertical velocity of about 2.350 km/s (Figure 5). Superimposed on the traces in Figure 3 are travel times computed in an isotropic model that matches the vertical velocities seen in the near-offset VSP data. It shows a significant underprediction of travel times for large offsets similar to what has been seen in other walkaway surveys, particularly in the North Sea [e.g., *Christie and Dangerfield*, 1987]. In fact, two of the four density-normalized moduli that determine propagation in a TIV medium for waves with polarization in the plane of the survey can be read directly from these data. A_{11} is the square of the horizontal P velocity which can be read as $\Delta X_s/\Delta T$ at the turning offsets in Figure 3. A_{33} is the square of the vertical P velocity which can be read as $\Delta Z_r/\Delta T$ in Figure 5. These axial P velocities differ by 12%. The remaining in-plane moduli (A_{55} and A_{13}) can be obtained by further analysis as described below.

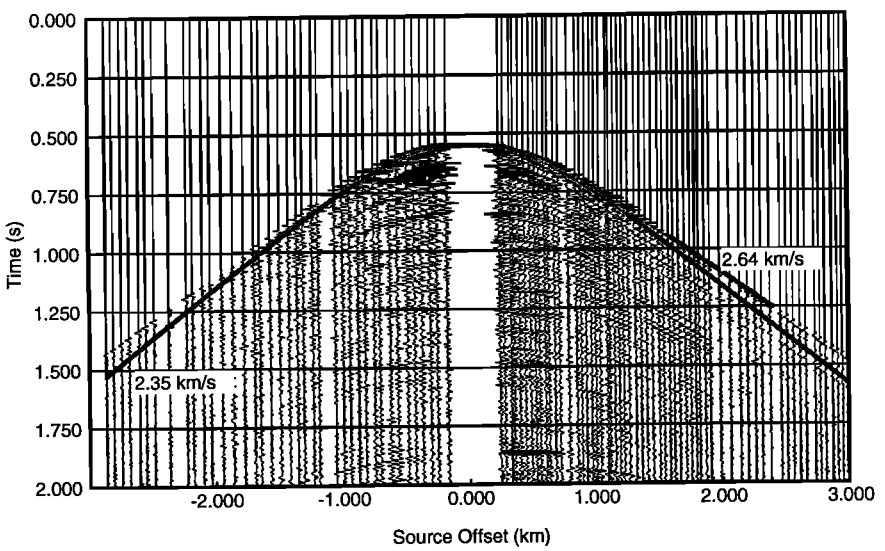

Figure 3. Vertical component common receiver gather for the central receiver at 1.008 km depth.

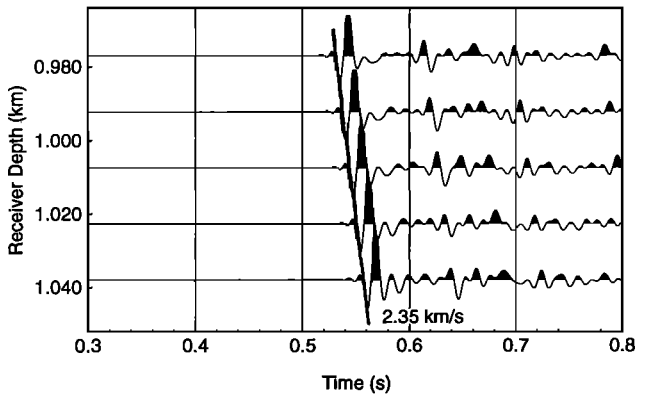

Figure 5. Vertical component common source gather for the source at −0.165 km offset from the well.

Anisotropic Elastic Moduli From Phase Velocity Analysis

Figure 6 shows a contour plot of picked first-break travel times as a function of source-receiver offset and receiver depth. It is a classical wave front chart. The essence of the phase velocity method is that at each point in the chart, the gradient of travel time is a point on the phase slowness surface for the medium at the given depth. The gradient of travel time has as components the apparent horizontal and vertical slowness of the direct qP arrival. Since our vertical receiver array is short, we will obtain phase points only for the medium at the center of the array (at 1.008 km). Since our horizontal source array is long and arrivals range from vertical to horizontal, we will sample the entire qP phase slowness surface at this depth and azimuth, obtaining about 200 estimated qP phase points.

Vertical Slowness as a Function of Offset

From each three-component trace, a two-component (vertical and radial) trace was created by rotating the coordinate system to align it with the horizontal polarization vector seen in the direct P arrival. Then, for each source position, vertical slownesses were estimated using the parametric inversion method described by *Esmersoy* [1990]. This method, applied to an array of two-component (vertical and radial) data windowed around the first arrival, finds a best fitting decomposition of the vector wave field as a sum of four plane waves (down and up, P and S), each with an associated polarization and slowness across the array. Figure 7 graphs the four vertical slownesses as a function of source offset. At large offsets, a one-plane wave model (for the direct qP arrival) was fit.

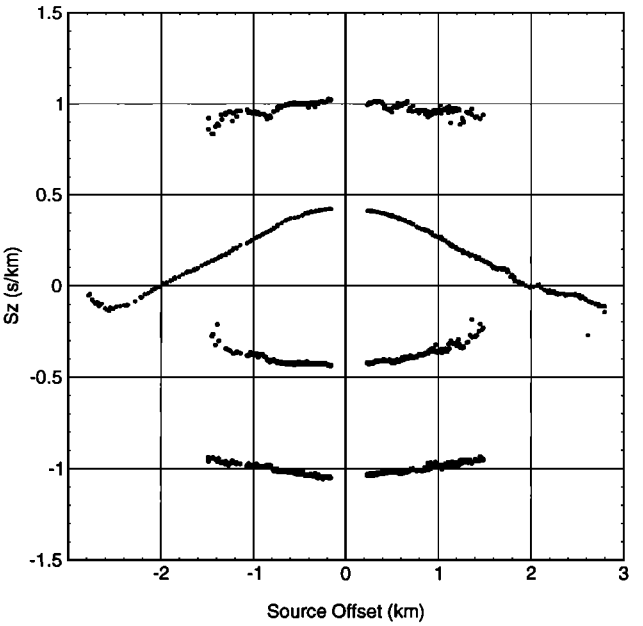

Figure 7. Vertical apparent slownesses calculated for each common source gather. From top to bottom they represent downgoing qSV, downgoing qP, reflected qP, and reflected qSV waves, respectively.

Horizontal Slowness as a Function of Offset

It was deemed inappropriate to attempt a parametric inversion for horizontal slownesses because there is some small variation in the picked travel times (presumably due to the fact that the data were acquired in two passes of the source boat). However, the overall trend of the data is surprisingly symmetric, with variation between the two sides of the survey having a magnitude similar to the level of local variation. Figure 8 shows travel time data from both sides of the survey plotted in squared travel time and offset coordinates. It is impossible to distinguish sets of points coming from the two sides of the survey. This is strong evidence that the layered-Earth assumption is valid.

Gaiser [1990] suggested calculating horizontal slownesses locally by fitting straight-line segments in the squared coordinate space. Given the large consistent data set, we found it practical instead to construct a smooth, symmetric global travel time function by fitting a third-degree polynomial in the squared domain. Offsets out to 2.800 km were used to help guarantee that the approximation would be smooth at offset 2.000 km. This approximating curve is superimposed on the data in Figure 8. The x derivative of the global travel time function gives horizontal slowness as a function of

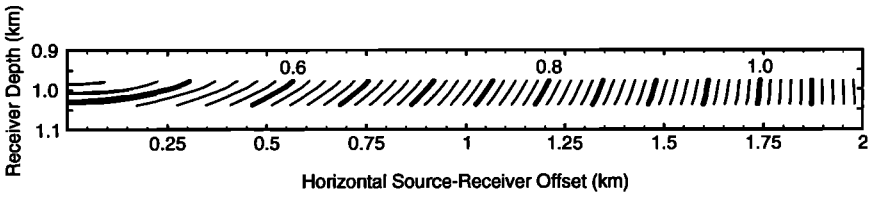

Figure 6. Wave front chart made from recorded first-break travel times.

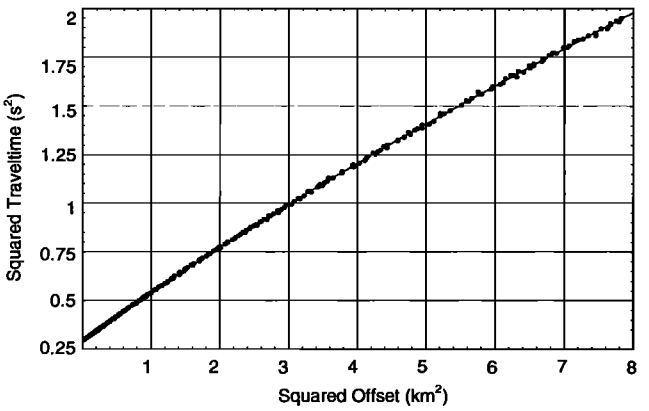

Figure 8. Squared qP travel time versus squared offset for the central receiver. A best fitting third-degree polynomial is superimposed on the data.

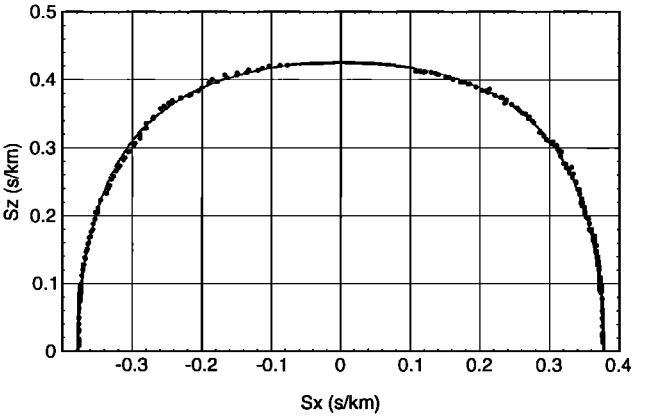

Figure 10. Estimated qP phase slowness points together with the analytic phase slowness curve for the best fitting TIV medium.

offset. It is shown in Figure 9 together with horizontal slownesses calculated locally using Gaiser's method.

Phase Slowness Surface and Anisotropic Moduli

At each source offset, the horizontal slowness calculated from the smooth curve displayed in Figure 9 was paired with the downgoing qP vertical slowness displayed in Figure 7 to define the two-component travel time gradient (i.e., the phase slowness vector) at that offset, at the depth of our central receiver. These phase slowness points are displayed in Figure 10 together with the analytic qP phase slowness curve for a TIV medium obtained as follows.

Miller and Spencer [this issue] show that given an estimate for A_{55}, the three remaining density-normalized moduli (A_{11}, A_{13}, A_{33}) can be directly estimated from qP phase slowness data. Since A_{55} is the square of the axial shear velocity, an estimate can be obtained from the wave field analysis data displayed in Figure 7. The points with maximum absolute slowness belong to near vertically propagating converted qSV waves. They show a slowness that lies between 1.02 and 1.07 s/km. It follows that A_{55} lies between 0.87 and 0.96 km^2/s^2. We used the value 0.91 in our calculations.

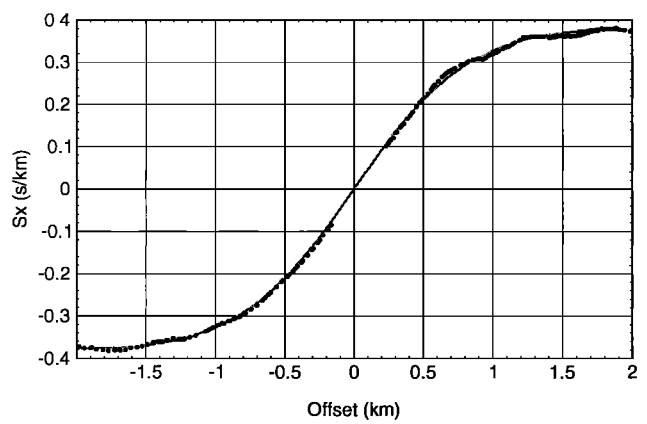

Figure 9. Horizontal apparent slowness calculated from the travel time data of Figure 8. The solid curve was obtained analytically from the curve shown in Figure 8 by differentiation and change of variables. The points shown were obtained by Gaiser's local method, fitting straight lines to 0.400-km segments of points in Figure 8.

Using this value for A_{55} and applying the method of *Miller and Spencer* [this issue] to the qP phase slowness points from Figure 10, we obtained elastic moduli $\{A_{11}, A_{13}, A_{33}, A_{55}\} = \{6.99, 2.64, 5.53, 0.91\}$. The analytic qP phase slowness curve from this model has been superimposed on the measured phase points in Figure 10. As measured by the relative error of the fit |measured phase-modeled phase|/modeled phase, the standard deviation of the scatter is 0.6%. Thus a conservative estimate is that the slownesses are fit to within ±1.5%. That implies a confidence in the estimated moduli of ±3%. Combining this with our earlier discussion of the confidence in A_{55}, we can tabulate

$$A_{11} = 6.99 \pm 0.21$$

$$A_{33} = 5.53 \pm 0.17$$

$$A_{qp} = 5.36 \pm 0.16$$

$$A_{55} = 0.91 \pm 0.05$$

$$A_{13} = 2.64 \pm 0.26.$$

Densities in the logged zone just below the survey lie in the range between 2200 and 2400 kg/m^3 with an average value close to 2300 kg/m^3.

Discussion

Figure 11 shows the impulse response from the inverted medium displayed in a form similar to that of Figure 1. In comparison to the Greenhorn shale of Figure 1, the Petronas shale shows a smaller degree of axial anisotropy as measured by the ratio V_{11}/V_{33} (1.12 for Petronas versus 1.23 for Greenhorn). However, Petronas shale shows a greater degree of anellipticity, with $(A_{11} + A_{33})/[2(A_{13} + 2A_{55})]$ equal to 1.40 for Petronas and 1.33 for Greenhorn. In terms of off-axis velocities the Petronas shale has $V_{qs}/V_{55} = 1.41$, $V_{qp}/[(A_{11} + A_{33})/2]^{1/2} = 0.93$. As noted earlier, the corresponding velocity ratios for the Greenhorn shale are 1.28 and 0.88.

As shown by *Miller and Spencer* [this issue], the goodness

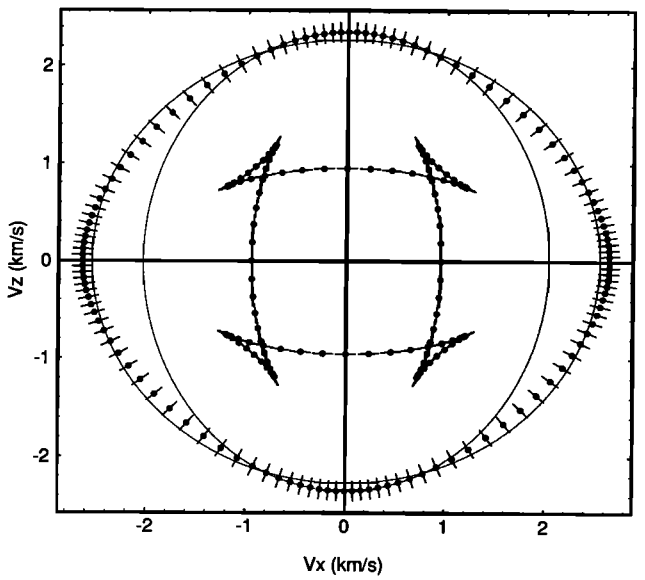

Figure 11. Impulse response of the estimated TIV medium. Superimposed are two ellipses calculated as the best elliptical approximations over phase angles from vertical to 30° and vertical to 90°, respectively.

of the fit to the *qP* phase points is essentially independent of the choice of A_{55}. For all values of A_{55} between 0.5 and 2.0, the best fitting medium shows a triplication in the *qSV* impulse response. This triplication is associated with strong anellipticity of the *qP* surface. Superimposed on Figure 11 are ellipses calculated as the best elliptical approximations over phase angles from vertical to 30° and 90°. The elliptical approximation at 90° significantly underestimates both the vertical and horizontal wave speeds. Figure 12 is a graph of the best fitting ellipticity (as measured by the ratio of vertical to horizontal semiaxis length) as a function of maximum phase angle from vertical to be fit. The range is from roughly 1.23 to 0.89 with a value of 1.0 at 55°. This medium confirms that ellipses make bad approximations to typical shale slowness or velocity surfaces [cf. *Thomsen*, 1986].

Miller and Spencer [this issue] also show that a good fitting TIV model in a single vertical plane would be expected even if the medium has azimuthal anisotropy induced by a vertical fracture system. Thus we cannot rule out the possibility that there is azimuthal anisotropy in this case. It would, however, be feasible to repeat this experiment in multiple azimuths to obtain data that could completely characterize a fractured TIV medium. *Miller and Spencer* [this issue] show that this could be done using as few as three correctly chosen survey directions.

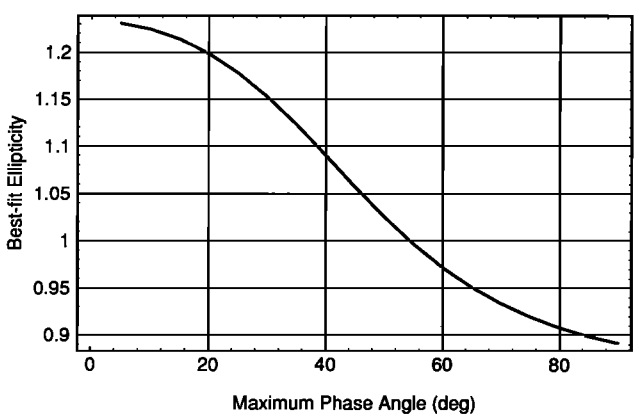

Figure 12. Best fitting ellipticity as (as measured by the ratio of vertical to horizontal semiaxis length) as a function of maximum phase angle from vertical to be fit.

It should also be pointed out that the parameters we have estimated represent an average "effective" medium at the scale of our seismic wavelengths (roughly the 0.100 km extent of our vertical array). It is evident from the logs that the actual medium shows considerable variation at a finer scale than that. We have verified numerically that the variation seen in the logs (Figure 2) would be grossly insufficient to account for the degree of measured anisotropy if the log values were taken to represent thin, isotropic layers (and assuming that the variation in the logged interval is representative of that in the zone just above it where we did our VSP). Thus the apparent anisotropy at the seismic scale would seem to represent a combination of a weak effect due to layering evident at the sonic scale with a strong effect due to the anisotropy of the material constituting the layers evident at the sonic scale. This is not surprising given ultrasonic measurements such as that of *Jones and Wang* [1981]. Clearly, it would be interesting to combine the methods described here with core measurements and with logs or crosswell measurements done at fine and intermediate scales.

Acknowledgments. The authors are grateful to Petronas for release of the data; to Roopa Gir for data acquisition; to John Walsh, Kai Hsu, and Leon Horowicz for helpful discussions; and to Nat Miller for programming the Mathematica anisotropy package that was used in making the analysis.

References

Ansel, E. A., Das Impulsfeld der practischen Seismik in graphischer Behandlung, *Gerlands Beitr. Geophys.*, *1*, 117–136, 1931.

Brodov, L. Y., V. I. Evstifeyev, E. V. Karus, and T. N. Kulichikhina, Some results of the experimental study of seismic anisotropy of sedimentary rocks using different types of waves, *Geophys. J. R. Astron. Soc.*, *76*, 191–200, 1984.

Byun, B. S., and D. Corrigan, Seismic traveltime inversion for transverse isotropy, *Geophysics*, *55*, 192–200, 1990.

Byun, B. S., D. Corrigan, and J. E. Gaiser, Anisotropic velocity analysis for lithology discrimination, *Geophysics*, *54*, 1564–1574, 1989.

Cholet, J., and H. Richard, A test on elastic anisotropy measurements at Berriane (North Sahara), *Geophys. Prospect.*, *2*, 232–246, 1954.

Christie, P., and J. Dangerfield, Borehole seismic profiles in the Ekofisk Field, *Geophysics*, *52*, 1328–1345, 1987.

Dellinger, J. A., Anisotropic seismic wave propagation, PhD. thesis, Stanford Univ., Stanford, Calif., 1991.

Dunoyer de Segonzac, P., and J. Laherrere, Application of the continuous velocity log to anisotropy measurements in northern Sahara: Results and consequences, *Geophys. Prospect.*, *7*, 202–217, 1959.

Esmersoy, C., Inversion of *P* and *SV* waves from multicomponent offset vertical seismic profiles, *Geophysics*, *55*, 39–50, 1990.

Gaiser, J. E., Transversely isotropic phase velocity analysis from slowness estimates, *J. Geophys. Res.*, *95*, 11,241–11,254, 1990.

Hagedoorn, J. G., The plus-minus method of interpreting seismic refraction sections, *Geophys. Prospect.*, *7*, 158–182, 1959.

Helbig, K., and M. Schoenberg, Anomalous polarization of elastic waves in transversely isotropic media, *J. Acoust. Soc. Am.*, *81*, 1235–1245, 1987.

Jolly, R. N., Investigation of shear waves, *Geophysics*, *21*, 905–938, 1956.

Jones, L. E. A., and H. F. Wang, Ultrasonic velocities in Cretaceous shales from the Williston basin, *Geophysics*, *46*, 288–297, 1981.

Meisner, R., Wavefront diagrams from uphole shooting, *Geophys. Prosp.*, *9*, 533–543, 1961.

Miller, D. E., and C. H. Chapman, Incontrovertible evidence of anisotropy in crosswell data, paper presented at the 61st Annual Meeting, Soc. of Explor. Geophys., Houston, Tex., 1991.

Miller, D. E., and C. Spencer, An exact inversion for anisotropic moduli from phase slowness data, *J. Geophys. Res.*, this issue.

Ricker, N., The form and laws of propagation of seismic wavelets, *Geophysics*, *18*, 10–40, 1953.

Schoenberg, M., and J. Douma, Elastic wave propagation in media with parallel fractures and aligned cracks, *Geophys. Prospect.*, *36*, 571–590, 1988.

Thomsen, L., Weak elastic anisotropy, *Geophysics*, *51*, 1954–1966, 1986.

Thornberg, H. R., Wavefront diagrams in seismic interpretation, *Am. Assoc. Pet. Geol. Bull.*, *14*(2), 185–200, 1930.

Vander Stoep, D. M., Velocity anisotropy measurements in wells, *Geophysics*, *31*, 900–916, 1966.

White, J. E., L. Martineau-Nicoletis, and C. Monash, Measured anisotropy in Pierre shale, *Geophys. Prospect.*, *31*, 709–725, 1983.

W. H. Borland, Schlumberger Overseas S.A., 907 Central Plaza Building, Phaholyothin Road, Bangkhen, Bangkok 10900, Thailand. (e-mail: borland@bkjm31.sinet.slb.com)

S. Leaney, Schlumberger Wireline and Testing, 10th Floor Wisma Rajawali Jalan Sudirman Kav. 34, P.O. Box 4895 JKT, Jakarta, Indonesia. (e-mail: leaney@sea601.sinet.slb.com)

D. E. Miller, Schlumberger-Doll Research, Old Quarry Road, Ridgefield, CT 06977-4108. (e-mail: miller@ridgefield.sdr.slb.com)

(Received June 28, 1993; revised July 5, 1994;
accepted July 14, 1994.)